Radiation Heat Transfer Across a Compressed Spheroidal Cavity

Sean P. Fitzgerald and William Strieder
Dept. of Chemical Engineering, University of Notre Dame, Notre Dame, IN 46556

Thermal radiation within enclosed pores is an important mode of heat transfer in numerous thermal engineering applications, such as void transport in high-temperature fire brick (Ganguley and Hasselman, 1976), cavity heat transfer in ceramic nuclear fuel elements (Marino, 1969, 1971), the passage of reaction heat during the high-temperature synthesis of advanced ceramic materials (Varma et al., 1990) and pore transport in reduced pressure, cryogenic insulation (Kaganer, 1969). In cases where the microstructural pore dimensions are small compared to the macroengineering lengths of the porous material, and the local temperature drop ΔT across the microstructural scale is small compared to the local average temperature $\overline{T}$, an effective conductivitiy λ_e can be rigorously formulated (Whitaker, 1980) and from this an average local radiation conductivity λ_r can be obtained. In a previous article (Fitzgerald and Strieder, 1997), a method was proposed to calculate useful equations for λ_r in model cavity shapes, based on a variational principle whose extremum value is the needed engineering property λ_e. As an appropriate trial function, the analytical solution of the corresponding two-phase Fourier heat-transfer problem with λ_s in the solid and a trial radiation conductivity λ_r^* in the specific model cavity shape was introduced. Upon substitution of the trial temperature into the variational integrals, a variational form was generated

$$\lambda_e \leq \lambda_e(\lambda_r^*), \tag{1}$$

and a λ_r^* was selected that gave the best (smallest) possible value of the variational effective conductivity for the heat-transfer calculation. Applied to radiation heat transfer down an elongated prolate spheroidal cavity, the variational method produced both a useful equation for λ_r^*, as well as a number of new exact results.

In this work, radiation heat transfer across an oblate spheroidal cavity in the direction of the axis of symmetry is considered. The cavity volume is generated by the revolution of an ellipse ($\rho^2 a^{-2} + z^2 b^{-2} = 1$) of semimajor axis a and semiminor axis b. However, revolution about the smaller axis b, rather than a as in the prolate case, generates a much different void volume, a compressed oblate spheroid. While the same eccentricity factor form characterizes the ellipse

$$\beta^2 = 1 - b^2 a^{-2}, \tag{2}$$

since b (oblate spheroid) refers to the symmetry axis and not a (prolate spheroid), its volumetric meaning for the two cases is much different, and the symbol β^2 rather than α^2 is used for the oblate spheroid cavity volume. The variational principle for λ_e, the trial temperature, the trial radiosity, the variational volume integrals, and the variational extremum calculations are all similar to the prolate case. With the caution that a and b are interchanged in the trial temperature, trial radiosity, and volume integrals, refer to the prolate calculation (Fitzgerald and Strieder, 1997) for details of the first part of the calculations. Consideration will begin with the variational result for the radiation void conductivity in terms of six surface integrals, which are different for the oblate void cavity. These forms will be given and their evaluation briefly outlined. The new oblate results will be discussed, and then compared with the prolate case.

Radiation Conductivity Across an Oblate Spheroid

Consider a large solid slab located between the planar surfaces Σ_- at $z = -L/2$ and Σ_+ at $z = +L/2$ at respective uniform temperatures T_+ and T_-, with a unit vector $\boldsymbol{k}$ pointing across the slab in the positive z-direction. Located at the slab center, $z = 0$ is an ellipsoidal void volume generated by rotating an ellipse, ($\rho^2 a^{-2} + z^2 b^{-2} = 1$), about its semiminor axis b. The oblate spheroidal cavity will then have its axis of symmetry in the direction of the applied temperature gradient $(T_+ - T_-)L^{-1}\boldsymbol{k}$. By definition, the effective conductivity λ_e in equality 1 is the ratio of the net heat flux Q across Σ_-, Σ_+ or any intermediate plane perpendicular to the z-axis to the absolute value of the applied gradient $\lambda_e (= QL|T_+ - T_-|^{-1})$. The void-solid interface Σ of the oblate spheroidal cavity has an average surface temperature $\overline{T}$ [$= (T_+ + T_-)/2$], and a surface normal $\boldsymbol{\eta}$ located at the point $\boldsymbol{r}$ on Σ that points away from the solid into the void volume. The surface

Correspondence concerning this article should be addressed to W. Strieder.

Σ emits and reflects radiation diffusely as a gray body with a local pointwise total hemispherical surface emissitivity $\epsilon(\bar{T})$, evaluated at the average temperature at the cavity surface. Σ follows Kirchoff's law (Siegel and Howell, 1992) absorbing the fraction ϵ of the radiation incident to a surface element on Σ, and diffusely reflecting the fraction $(1-\epsilon)$.

Since the objective is to obtain the void radiation conductivity λ_r or its best variational estimate λ_r^* for radiative heat transfer down along the symmetry axis, only surface to surface element radiative transport will be considered. The differential view factor $K(\boldsymbol{r},\boldsymbol{r}')d^2\boldsymbol{r}$ gives the fraction of radiation, diffusely distributed, leaving a unit surface element located at $\boldsymbol{r}'$ on Σ, that travels a straight line free path and arrives at a second surface element $d^2\boldsymbol{r}$ at $\boldsymbol{r}$ on Σ. As discussed in the introduction, we can begin with the variational void radiation conductivity, similar in form to Eq. 51 in the prolate cavity article (Fitzgerald and Strieder, 1997)

$$\frac{\lambda_r^*}{Cb}=\frac{\chi_0\lambda_0(\chi_2+\lambda_2)-\chi_0\lambda_1^2-\chi_1^2\lambda_0}{(\chi_0+\lambda_0)(\chi_2+\lambda_2)-(\chi_1+\lambda_1)^2} \tag{3}$$

where $C=4\sigma\bar{T}^3$ and σ is the Stefan-Boltzmann constant.

In general, each of the first three surface integrals (χ_0, χ_1, χ_2) can be written in the form

$$\Lambda_{i,j}=\Sigma^{-1}\int_\Sigma d^2\boldsymbol{r}(\boldsymbol{k}\cdot\boldsymbol{r}/b)^i(\boldsymbol{k}\cdot\boldsymbol{\eta})^j \quad (i,j=0,1,2) \tag{4}$$

or in terms of the elliptical arc length ds and coordinates ρ, z

$$\Lambda_{i,j}=2\pi\Sigma^{-1}\int_{-b}^{b}dz\,\rho[ds/dz](z/b)^i(\eta_z)^j. \tag{5}$$

In Eq. 5, the integration over the angle of revolution ϕ produced the prefactor 2π. For an oblate spheroidal cavity generated by the rotation of $\rho^2a^{-2}+z^2b^{-2}=1$ about the semiminor axis b, the cavity volume is

$$V_\phi=4\pi ba^2/3, \tag{6}$$

the component of the surface normal $\boldsymbol{\eta}$ along the symmetry axis is

$$\eta_z=-zb^{-2}(\rho^2a^{-4}+z^2b^{-4})^{-1/2}, \tag{7}$$

the rate of change of the arc length coordinate along the symmetry axis is

$$ds/dz=(1+z^2\rho^{-2}a^4b^{-4})^{1/2}, \tag{8}$$

and the radial coordinate of the oblate spheroidal cavity volume is

$$\rho=a(1-z^2b^{-2})^{1/2}. \tag{9}$$

With the substitution of Eqs. 7–9 into Eq. 5, the $\Lambda_{i,j}$ integrals can be done exactly. The oblate spheroidal cavity void-solid interface area Σ is obtained from Eq. 5 with $i=j=0$

$$\Lambda_{0,0}=1 \tag{10}$$

or

$$=2\pi b^2\Sigma^{-1}\left\{(1-\beta^2)^{-1}+(2\beta)^{-1}\ln[(1+\beta)/(1-\beta)]\right\}. \tag{11}$$

Then, with the oblate spheroidal surface area (Eq. 11), volume (Eq. 6), as well as Eqs. 5 and 7–9, the χ_0 integral

$$\chi_0=(b\Sigma/V_\phi)\epsilon(1-\epsilon)^{-1}\Lambda_{2,0} \tag{12}$$

becomes

$$\chi_0=\frac{3}{8}\frac{\epsilon}{(1-\epsilon)}\frac{1}{\beta^2}\left\{1+\beta^2-\frac{(1-\beta^2)^2}{2\beta}\ln\left(\frac{1+\beta}{1-\beta}\right)\right\}; \tag{13}$$

the χ_1 integral

$$\chi_1=(b\Sigma/V_\phi)\epsilon(1-\epsilon)^{-1}\Lambda_{1,1}, \tag{14}$$

has the form

$$\chi_1=-\epsilon(1-\epsilon)^{-1}; \tag{15}$$

and the χ_2 integral

$$\chi_2=(b\Sigma/V_\phi)\epsilon(1-\epsilon)^{-1}\Lambda_{0,2}, \tag{16}$$

is given by

$$\chi_2=\frac{3}{2}\frac{\epsilon}{(1-\epsilon)}\frac{1}{\beta^2}\left\{1-\frac{(1-\beta^2)}{2\beta}\ln\left(\frac{1+\beta}{1-\beta}\right)\right\}. \tag{17}$$

The λ integrals require a form for the one-dimensional (1-D) kernel $K(z,z')$ for transport within an oblate spheroidal cavity from the surface slice Σ_{dz}, the cavity area cut by the differential dz, to the surface element $\Sigma_{dz'}$ corresponding to dz'

$$dzdz'\,K(z,z')=\int_{\Sigma_{dz}}d^2\boldsymbol{r}\int_{\Sigma_{dz'}}d^2\boldsymbol{r}'\,K(\boldsymbol{r},\boldsymbol{r}'). \tag{18}$$

This 1-D form can be generated directly from the prolate kernel by the interchange of a and b (Fitzgerald and Strieder, 1997)

$$K(z,z')/\pi=1+\beta^2|z-z'|\{2b^2(4-3\beta^2)+\beta^4(z-z')^2+6\beta^2zz'\}\{4b^2(1-\beta^2)+\beta^4(z+z')^2+4\beta^2(1-\beta^2)zz'\}^{-3/2}. \tag{19}$$

The first λ integral

$$\lambda_0 = (2bV_\phi)^{-1} \int_\Sigma d^2r \int_\Sigma d^2r'\, K(r,r')[k\cdot(r'-r)]^2, \quad (20)$$

can be written in the 1-D form from the oblate kernel 1-D Eqs. 18 and 19

$$\lambda_0 = (2bV_\phi)^{-1} \int_{-b}^{b} dz \int_{-b}^{b} dz'\, K(z,z')[z'-z]^2, \quad (21)$$

and from Eqs. 6 and 19 its analytical form is

$$\lambda_0 = \frac{3}{2}\frac{1}{\beta^2}\left\{1 - \frac{(1-\beta^2)}{2\beta}\ln\left(\frac{1+\beta}{1-\beta}\right)\right\}. \quad (22)$$

The second λ integral

$$\lambda_1 = (2V_\phi)^{-1} \int_\Sigma d^2r \int_\Sigma d^2r'\, K(r,r') \times [k\cdot(r'-r)][k\cdot(\eta'-\eta)], \quad (23)$$

where η' is the surface normal evaluated at r' on Σ, and with the 1-D kernel definition (Eq. 18), along with Eqs. 6 and 7

$$\lambda_1 = \frac{3(1-\beta^2)^{1/2}}{8\pi b^3} \int_{-b}^{b} dz \int_{-b}^{b} dz'\, K(z,z')[z'-z] \times \left[\frac{z}{\left(b^2+\beta^2 z^2(1-\beta^2)^{-1}\right)^{1/2}} - \frac{z'}{\left(b^2+\beta^2(z')^2(1-\beta^2)^{-1}\right)^{1/2}}\right]. \quad (24)$$

Finally, the third λ integral

$$\lambda_2 = b(2V_\phi)^{-1} \int_\Sigma d^2r \int_\Sigma d^2r'\, K(r,r')[k\cdot(\eta'-\eta)]^2 \quad (25)$$

with Eqs. 6, 7 and 18 becomes

$$\lambda_2 = \frac{3}{8\pi b^2} \int_{-b}^{b} dz \int_{-b}^{b} dz'\, K(z,z') \times \left[\frac{z}{\left(b^2+\beta^2 z^2(1-\beta^2)^{-1}\right)^{1/2}} - \frac{z'}{\left(b^2+\beta^2(z')^2(1-\beta^2)^{-1}\right)^{1/2}}\right]^2 \quad (26)$$

Conclusion and Discussion

The $\lambda_r^*(Cb)^{-1}$ expression (Eq. 3), with χ's and λ's specified, respectively, by Eqs. 15, 17, 19, 22, 24, and 25, provides from Eq. 1 a best estimate of λ_e, as well as a variational upper bound. The $\lambda_e(\lambda_r^*)$ expression is found to be (Fitzgerald and Strieder, 1997) the λ_e of the corresponding two-Fourier phase problem, that is, the exact solution for the same geometry with a solid conductivity λ_s and an oblate spheroid with model, void radiation, Fourier conductivity λ_r^*. Each χ (Eqs. 15, 17, and 19) has the form of the emissivity factor $\epsilon(1-\epsilon)^{-1}$ times either an analytical function of the eccentricity β, or a constant. The λ_0, λ_1 and λ_2 terms (Eqs. 22, 24, and 26) depend only on the cavity shape through β. The first λ_0 is given by the analytical Eq. 22. The other two integrals, λ_1 and λ_2 (Eqs. 24 and 26, respectively), are evaluated by three-point Newton-Cotes quadrature methods (Ralston and Rabinowitz, 1978). Plots of λ_0, λ_1, and λ_2 vs. the eccentricity squared β^2 are shown in Figure 1. Once λ_1 and λ_2 are done for the compressed spheroid cavity eccentricity range from 0 to 1, the dimensionless void radiation conductivity model is specified for all ϵ and β^2.

In Figure 2, $\lambda_r^*(Cb)^{-1}$ is plotted vs. the surface emissivity ϵ for various degrees of compression from the sphere cavity ($\beta^2 \to 0$) to the thin discus, flattened spheroid limit ($\beta^2 \to 1$). The surface of Figure 2 demonstrates the overall behavior of $\lambda_r^*(Cb)^{-1}$ for an oblate spheroidal cavity, as well as the four possible limits, $\beta^2 \to 0$, $\beta^2 \to 1$, $\epsilon \to 0$, and $\epsilon \to 1$. Figure 2 also lists the parallel plate curve for comparison. For the sphere limit, $\beta^2 \to 0$, it is necessary to expand Eq. 3 for $\lambda_r^*(Cb)^{-1}$ in β^2 for arbitrary emissivity ϵ. The first nonzero term in both the expansions of the numerator and the denominator of Eq. 3 are of the order β^4 and their ratio gives the limit

$$\lim_{\beta^2 \to 0} \lambda_r^*(Cb)^{-1} = \epsilon \qquad \text{(spherical void)}, \quad (27)$$

shown as the lefthand edge of the shaded surface of Figure 2. In this limit the trial forms used for the temperature and radiosity are known to be the exact results (Tsai and Strieder, 1985; Fitzgerald and Strieder, 1997).

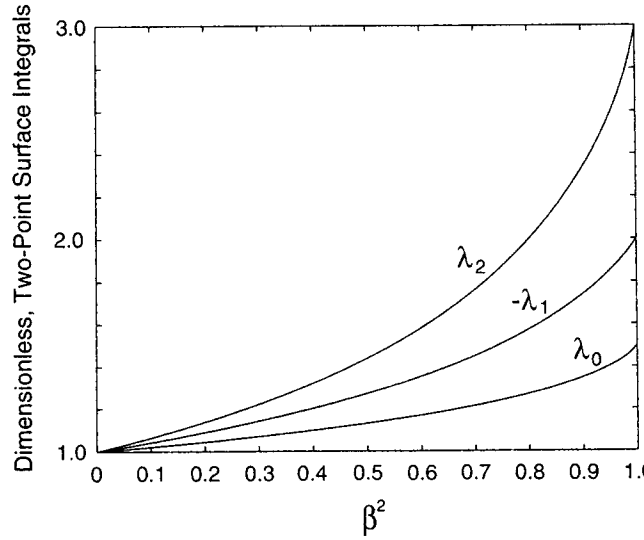

Figure 1. Values of λ_0, $-\lambda_1$ and λ_2, respectively from Eqs. 22, 24, and 26 vs. oblate spheroid eccentricity squared β^2.

Note that λ_1 is always negative and the corresponding positive value ($-\lambda_1$) is shown here.

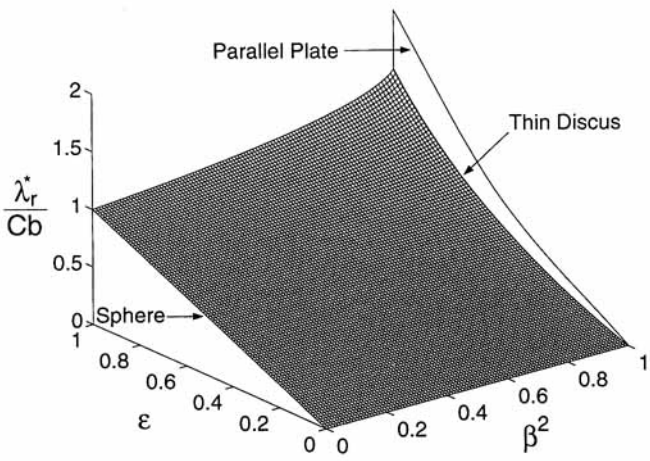

Figure 2. Dimensionless radiation thermal conductivity $\lambda_r^*(Cb)^{-1}$ vs. the surface emissivity ϵ and oblate spheroid squared eccentricity β^2 is given as the shaded surface.

The single curve at the back is the corresponding $\lambda_r^*(Cb)^{-1}$ for parallel plates separated by a distance $2b$.

In the opposite limit $\beta^2 \to 1$ of a thin discus oblate spheroid, the righthand side of Figure 1 provides the limits $\lambda_0 \to 3/2$, $\lambda_1 \to -2$ and $\lambda_2 \to 3$. Also from Eqs. 13, 17, 15, and 3, we have, respectively, the limits $\chi_0 \to 3\epsilon(4-4\epsilon)^{-1}$, $\chi_2 \to 3\epsilon(2-2\epsilon)^{-1}$ as $\beta^2 \to 1$; the equality $\chi_1 = -\epsilon(1-\epsilon)^{-1}$; and the limit

$$\lim_{\beta^2 \to 1} \lambda_r^*(Cb)^{-1} = \frac{3}{2}\epsilon(2-\epsilon)^{-1}$$

(oblate spheroid, thin discus void), (28)

seen at the righthand edge of the $\lambda_r^*(Cb)^{-1}$ surface in Figure 2. This result is reminiscent of the flux Q between two parallel plates (Bird et al., 1960) linearized in the dimensionless temperature drop $(\Delta T/\bar{T})$ across the plates $[Q = -\epsilon(2-\epsilon)^{-1}C\Delta T]$, and the associated radiation void conductivity between two parallel plates separated by a distance $2b$

$$\lambda_r^*(Cb)^{-1} = 2\epsilon(2-\epsilon)^{-1} \quad \text{(parallel plate model void)}. \quad (29)$$

The compressed oblate discus limit (Eq. 28) in Figure 2 is smaller than the parallel plate result (Eq. 29) by a factor of 0.75. To develop the relationship between these conductivities, we consider two parallel, directly opposed, identical planar rings a distance $2z$ apart, each with an elemental radius from ρ to $\rho + d\rho$. In the thin discus limit, the inequalities $d\rho \gg 2b > 2z$ hold, and radiation diffusely leaving a $d\rho$ ring will be absorbed after a number of plate to plate free paths into either the original emitting $d\rho$ ring or its $d\rho$ mirror image. This is because radiation diffusely leaving the surface will travel, on the average, *laterally* about one plate spacing $2z$ for each free path, but the $d\rho$ ring is much wider than the maximum plate spacing dimension $2b$. This permits the use of the parallel plate Eq. 29 for the void radiation conductivity between the $d\rho$ ring and its mirror $d\rho$ ring, but with b replaced by the local value z for $d\rho$. If, as we move along the radial dimension ρ from 0 to a, the plate spacing $2z$ varies from $2b$ to 0 according to Eq. 9, the compressed oblate void is generated. The volume average of the conductivity (Eq. 29) over this oblate spheroid gives exactly the Eq. 28 for the compressed oblate, thin discus, axial radiation conductivity.

The ϵ dependence of $\lambda_r^*(Cb)^{-1}$ in Eq. 3 is entirely contained in χ_0, χ_1 and χ_2, each with a factor $\epsilon(1-\epsilon)^{-1}$. For a black body surface ($\epsilon \to 1$), the χ's approach infinity as $\epsilon(1-\epsilon)^{-1}$ and

$$\lim_{\epsilon \to 1} \lambda_r^*(Cb)^{-1} = \lambda_0 \quad (30)$$

The β form of λ_0, given by Eq. 22, can be regarded as a very good approximation of the axial radiation conductivity for an oblate ellipsoid with black surfaces. The β dependence of λ_0 can be seen at the back side of the surface in Figure 2. The dimensionless variational radiation conductivity across a black oblate cavity varies in a slow, monotone fashion from unity at $\beta^2 = 0$ up to 1.5 at $\beta^2 = 1$.

In the neighborhood of the perfectly reflecting surface ($\epsilon \to 0$), the behavior of the radiation void conductivity is given by the front of the Figure 2 surface. The χ's, from their $\epsilon(1-\epsilon)^{-1}$ factor, become very small, the conductivity $\lambda_r^*(Cb)^{-1}$ of Eq. 3 vanishes for all β^2 values, and

$$\lim_{\epsilon \to 0} \frac{\lambda_r^*}{\chi_0 Cb} = 1. \quad (31)$$

Equation 31 predicts that $\lambda_r^*(Cb)^{-1}$ increases from zero for any β^2, with an initial ϵ slope $\chi_0(1-\epsilon)\epsilon^{-1}$ given by Eq. 13. This slope decreases monotonically with β^2 from unity for a spherical cavity with no compression ($\beta^2 \to 0$), until it drops to a value of 0.75 for void radiation heat transfer across a flattened discus, oblate spheroid ($\beta^2 \to 1$). Since $\lambda_r^*(Cb)^{-1} = 0$ at $\epsilon = 0$ for all β^2, the sphere will have a dimensionless conductivity larger than the compressed discus at lower emissivities, $\epsilon < 0.5$. From Eqs. 27 and 28, we see that the $\lambda_r^*(Cb)^{-1}$ values at the extremes, $\beta^2 \to 0$ and $\beta^2 \to 1$, are equal at $\epsilon = 0.5$, and cross over for $\epsilon > 0.5$. Finally at $\epsilon = 1$, $\lambda_r^*(Cb)^{-1}$ is only 1 for the sphere ($\beta^2 \to 0$), but is now larger, 3/2, for the dimensionless axial radiation conductivity of the oblate thin discus ($\beta^2 \to 1$). Unlike the prolate spheroid which exhibits rapid increases (see Figure 3b of Fitzgerald and Strieder, 1997) in $\lambda_r^*(Cb)^{-1}$ near the elongation limit ($\alpha^2 \to 1$), near the compression limit ($\beta^2 \to 1$) of an oblate spheroid a mild increase occurs for a fixed ϵ between $0.5 < \epsilon < 1$ with a slight decrease for $0 < \epsilon < 0.5$.

The dimensionless coefficient of void thermal radiation conductivity (Eq. 3) down the symmetry axis of an oblate spheroid has been obtained. Physically justifiable results are obtained in the neighborhood of low emissivity $\epsilon \to 0$ for any β^2, the sphere limit $\beta^2 \to 0$ for any ϵ, and for a flattened disk oblate spheroidal cavity $\beta^2 \to 1$ for any ϵ. One consequence of using the two-phase Fourier engineering model concept of a solid and void radiation conductivity to formulate the trial temperature and radiosity, as has been done here, is that the final results can be readily cast in terms of current engineering models that use radiation conductivities in process calculations.

Notation

$d^2\boldsymbol{r}$ = differential area located at the point $\boldsymbol{r}$ on the surface of Σ
ds = differential ellipsoid arc length
dz = differential along the axis of symmetry
$\boldsymbol{k}$ = Cartesian unit vector pointing across the solid from $z = -L/2$ to $z = L/2$
$K(z, z')\,dz\,dz'$ = 1-D kernel, defined in Eq.18
L = slab thickness
Q = net heat flux across plane of the slab in the z-direction per unit surface area
$\boldsymbol{r}$ = location vector pointing from the spheroid center
T_-, T_+ = temperatures at $z = -L/2$ on Σ_- and $z = +L/2$ on Σ_+, respectively
$\bar{T}$ = average slab temperature, $(T_+ + T_-)/2$
V_ϕ = volume of the ellipsoidal cavity
z, z = Cartesian coordinate vector and magnitude running from $-L/2$ to $L/2$

Greek letters

α^2 = square of the prolate spheroid eccentricity
β^2 = square of the oblate spheroid eccentricity
ϵ = surface emissivity
$\boldsymbol{\eta}(\boldsymbol{r})$ = surface normal vector pointing away from the solid at the point $\boldsymbol{r}$
η_z = z-component of vector $\boldsymbol{\eta}$
λ_r, λ_r^* = average void radiation thermal conductivity and the variational optimum value in Eq. 3
λ_s = thermal conductivity of the solid
$\lambda_0, \lambda_1, \lambda_2$ = defined and evaluated in Eqs. 20–27
$\Lambda_{i,j}$ = Eqs. 4 and 5, $(i, j = 0, 1, 2)$
σ = Stefan-Boltzmann constant
Σ = cavity-solid interfacial area
Σ_-, Σ_+ = planar solid surfaces at $z = -L/2$ and $z = +L/2$, respectively

Literature Cited

Bird, R. B., W. E. Stewart, and E. N. Lightfoot, *Transport Phenomena*, Wiley, New York, p. 446 (1960).

Fitzgerald, S. P., and W. Strieder, "Radiation Heat Transfer down an Elongated Spheroidal Cavity," *AIChE J.*, **43**, 2 (1997).

Ganguley, B. K., and D. P. H. Hasselman, "Effect of Matrix Conductivity on the Radiation Heat Transfer Across Spherical Pores," *J. Amer. Ceram. Soc.*, **59**, 83 (1976).

Kaganer, M. G., *Thermal Insulation in Cryogenic Engineering*, IPST Press, Jerusalem (1969).

Marino, G. P., "Radiation Transfer Across a Spherical Pore in a Linear Temperature Gradient," *Trans. AIME*, **245**, 821 (1969).

Marino, G. P., "The Porosity Correction Factor for the Thermal Conductivity of Ceramic Fuels," *J. Nucl. Mat.*, **38**, 178 (1971).

Ralston, A., and P. Rabinowitz, *A First Course in Numerical Analysis*, McGraw-Hill, New York (1978).

Siegel, R., and J. R. Howell, *Thermal Radiation Heat Transfer*, 3rd ed., McGraw-Hill, New York (1992).

Tsai, D. S., and W. Strieder, "Radiation Across a Spherical Cavity having both Specular and Diffuse Reflectance Components," *Chem. Eng. Sci.*, **41**, 170 (1985).

Varma, A., G. Cao, and M. Morbidelli, "Self-Propagating Solid-Solid Noncatalytic Reactions in Finite Pellets," *AIChE J.*, **36**, 1039 (1990).

Whitaker, S., "Radiant Energy Transport in Porous Media," *I.&E.C. Fundam.*, **19**, 210 (1980).

Manuscript received Feb. 20, 1997, and revision received May 27, 1997.